vibration

MDPI

Article

The Control of an Active Seat Suspension Using an Optimised Fuzzy Logic Controller, Based on Preview Information from a Full Vehicle Model

Abdulaziz Alfadhli *, Jocelyn Darling and Andrew J. Hillis

Centre for Power Transmission and Motion Control, Department of Mechanical Engineering, University of Bath, Claverton Down, Bath BA2 7AY, UK; J.Darling@bath.ac.uk (J.D.); a.j.hillis@bath.ac.uk (A.J.H.)

* Correspondence: a.alfadhli@bath.ac.uk

Received: 15 December 2017; Accepted: 6 February 2018; Published: 9 February 2018

Abstract: The use of suspension preview information obtained from a quarter vehicle model (QvM) to control an active seat has been shown by the authors to be very promising, in terms of improved ride comfort. However, in reality, a road vehicle will be subjected to disturbances from all four wheels, and therefore the concept of preview enhanced control should be applied to a full vehicle model. In this paper, different preview scenarios are examined, in which suspension data is taken from all or limited axles. Accordingly, three control strategies are hypothesized—namely, front-left suspension (FLS), front axle (FA), and four wheel (4W). The former utilises suspension displacement and velocity preview information from the vehicle suspension nearest to the driver's seat. The FA uses similar preview information, but from both the front-left and front-right suspensions. The 4W controller employs similar preview information from all of the vehicle suspensions. To cope with friction non-linearities, as well as constraints on the active actuator displacement and force capabilities, three optimal fuzzy logic controllers (FLCs) are developed. The structure of each FLC, including membership functions, scaling factors, and rule base, was sequentially optimised based on improving the seat effective amplitude transmissibility (SEAT) factor in the vertical direction, using the particle swarming optimisation (PSO) algorithm. These strategies were evaluated in simulation according to ISO 2631-1, using different road disturbances at a range of vehicle forward speeds. The results show that the proposed controllers are very effective in attenuating the vertical acceleration at the driver's seat, when compared with a passive system. The controller that utilised suspension preview information from all four corners of the car provided the best seat isolation performance, independent of vehicle speed. Finally, to reduce the implementation cost of the "four suspension" controller, a practical alternative is developed that requires less measured preview information.

Keywords: active seat suspension; optimum fuzzy logic control; preview information; full vehicle model

1. Introduction

Vehicle drivers are frequently exposed to vertical vibration over a low frequency range, which is transmitted to the driver's seat from road roughness through the vehicle suspension and body. This vibration reduces ride comfort and can cause long-term health problems, as the human body is most sensitive to vertical vibration in the frequency range of 4–8 Hz [1,2]. Consequently, seat suspensions are practicable and cost-effective solutions that are used in vehicles to overcome these effects.

Three configurations of seat suspension exist in this field: passive, semi-active, and active. Passive systems are simple and cost-effective, consisting of spring and damper elements with fixed characteristics. Due to this, they have limited vibration attenuation performance. Semi-active suspensions

are also comprised of spring and damper elements, but the properties of these elements can be adjusted using minimal power consumption. Thus, their vibration attenuation performance is superior to passive systems. However, their performance is still compromised, because they can only dissipate energy from the system [3]. Conversely, active seat suspensions, which apply an external force based upon a control strategy, can significantly reduce vibration over a broadband frequency range, and therefore can be considered as an alternative to costly vehicle active suspension systems that are called upon to optimise both ride comfort and handling.

One of the essential features of active suspensions is the control strategy and many control strategies have been investigated in the literature, such as optimal control [4], H-infinity [5–7], adaptive filtered-x LMS [8,9], sliding mode control [10–12], neural network control [13], fuzzy logic control (FLCs) [14–20] and preview control [21–29].

It was Bender who first presented the concept of preview information in vehicle suspensions [30], suggesting that employing preview information can effectively improve vehicles' performance. Preview information from the road disturbance is used in the control approach, before the road disturbances act on the vehicle body. This approach can decrease the controller and actuator response times, hence improving the suspension performance [31,32]. There are two approaches to preview control. The first is "look ahead", where the road disturbances are sensed as preview information for the controller of the active suspension, before these disturbances act on the vehicle. The second is the "wheelbase", where instead of acquiring preview information from the road disturbances, the disturbances are sensed from the dynamic changes of the front wheels, and later used as preview information to control the active rear suspension. However, both approaches have some drawbacks; for instance, the real implementation of the look-ahead approach is costly and complicated, as it requires expensive sensory systems to accurately predict road profiles [27,31,32]. Whilst the "wheelbase" option seems more practical than the "look ahead" alternative, the preview information is only accessible to control the rear suspension, and road excitations at the rear axle cannot be always correctly predicted from those encountered by the front axle, especially during cornering [33]. In a previous study by the authors [34], a simple and cost-effective controller approach with a linear Quarter Vehicle Model (QvM), which uses preview information from the vehicle suspension, was applied to control an active seat suspension. Both simulation and experimental results showed that this approach can significantly attenuate the vertical vibration at the driver's seat. To make the application more realistic and investigate the benefits that could be gained from this principle, a full vehicle model is utilised here. To cope with vehicle suspension non-linearities and physical constraints in both the seat suspension travel and actuator force capacity, a fuzzy logic control (FLC) approach was used. One of the main drawbacks of FLC is the construction of the rule base (RB) and the fuzzification process, including membership functions (MFs) and scaling factors. Moreover, there is no standard method to set the number and type of the MFs. In addition, the RB depends on expert knowledge about the system behaviour, which is influenced by the type and number of both the input and output variables, as well as their corresponding scaling factors. It is challenging to hypothesise the RB for a complicated system [35], such as that required for an active seat suspension. A trial and error approach has been widely used to tune either the parameters of the MFs or the scaling factors under a suggested RB [14,15,18], but this is both time-consuming and an inefficient way of finding a global optimum solution [36].

In contrast, other researchers have used evolution optimisation algorithms, such as genetic algorithms (GA) [37–39] or the Particle Swarm Optimisation (PSO) algorithm [16,35,40]. Rajeswari and Lakshmi [41] employed both GA and PSO to optimise the scaling factors, MFs and RB of an FL controller for an active suspension system. They concluded that the PSO is more effective in optimising the FLC structure when compared with the GA. The PSO technique is simple and can be easily applied. Moreover, its convergence characteristics are stable and computationally efficient [42–44].

This paper presents the design of three optimal FL controllers for an active seat suspension, which use measurable and low-cost preview information from the vehicle suspension states,

considering hard constraints related to both allowable seat stroke and actuator force capacity. These controllers are front-left suspension (FLS-FLC), front axle (FA-FLC), and four wheels (4W-FLC). The first utilises suspension displacement and velocity information from the nearest corner to the active seat. The FA-FLC uses similar preview information, but from both the front left and right suspensions. The 4W-FLC, employs preview information from all four vehicle suspensions. The optimal structure of each of the FLCs, including the MFs, scaling factors, and RB were sequentially designed using PSO.

1.1. Integrated Model

The vehicle and seat simulation model used in this study consists of a full linear vehicle model, a passive seat suspension, and a driver's body model, as shown in Figure 1. The full vehicle model is the "seven degree of freedom" model presented in [45]. The vehicle body mass M_s (sprung mass) is assumed to be a rigid body with bounce, pitch, and roll motions denoted by x_s, θ, and ϕ, respectively. In this study, we have neglected any lateral or yaw body motions that would be appropriate in the analysis of vehicle handling.

Each wheel of the front and rear axles, represented by the un-sprung masses m_{11}, m_{12}, m_{21}, and m_{22}, has a single degree of freedom in the vertical direction, denoted by x_{11}, x_{12}, x_{21}, and x_{22}, respectively, while the road disturbances at these wheels are represented by x_{r11}, x_{r12}, x_{r21}, and x_{r22}. For simplicity, this model involves only the driver's seat, with a linear lumped mass-spring-damper of one degree of freedom (DOF) in the vertical direction, denoted by x_{se}. Further development of the model could include the extension of this study to multiple suspension seats, where the cross coupling would be explicitly modelled. Moreover, the driver's body is represented by a one DOF in the vertical direction, denoted by x_b. The tyre springs and suspension spring elements of the front and rear axles are presumed to be linear. Assuming small pitch and roll angles, the dynamic equations of the integrated model are given as follows:

(1) Vehicle body motion:

(a) Bounce

$$M_s\ddot{x}_s = -\left[\sum_{i,j=1,2} F_{sij} + f\left(V_{sij}\right)\right] + F_{se} + F_a \tag{1}$$

where F_{sij} is the suspension dynamic force at each vehicle suspension, given by:

$$F_{sij} = k_{sij}\left(x_{sij} - x_{ij}\right) + c_{sij}\left(\dot{x}_{sij} - \dot{x}_{ij}\right),\ i = 1,2\ \&\ j = 1,2 \tag{2}$$

while $f\left(V_{sij}\right)$ is the dry friction force of the suspension damper at each wheel, F_{se} is the seat suspension force, and F_a is the controller force.

(b) Pitch

$$I_{sy}\ddot{\theta} = L_f(F_{s11} + F_{s12} + f(V_{s11}) + f(V_{s12})) - L_r(F_{s21} + F_{s22} + f(V_{s21}) + f(V_{s22})) - R_x(F_{se} + F_a) \tag{3}$$

(c) Roll

$$I_{sx}\ddot{\phi} = b(F_{s12} + F_{s22} + f(V_{s12}) + f(V_{s22})) - a(F_{s11} + F_{s21} + f(V_{s11}) + f(V_{s21})) + R_y(F_{se} + F_a) \tag{4}$$

(2) Un-sprung masses

$$m_{ij}\ddot{x}_{ij} = F_{sij} + f\left(V_{sij}\right) - k_{tij}\left(x_{ij} - x_{rij}\right)\ i,j = 1\ \&\ 2 \tag{5}$$

(3) Seat suspension

$$F_{se} = k_{se}\left(x_{se} - x_{sp}\right) + c_{se}\left(\dot{x}_{se} - \dot{x}_{sp}\right) \tag{6}$$

$$m_{se}\ddot{x}_{se} = -(F_{se} + F_a) - k_b(x_{se} - x_b) - c_b\left(\dot{x}_{se} - \dot{x}_b\right) \tag{7}$$

(4) Driver's body

$$m_b\ddot{x}_b = k_b(x_{se} - x_b) + c_b(\dot{x}_{se} - \dot{x}_b) \quad (8)$$

Each of the vehicle suspension dampers includes a non-linear dry friction force $f(V_s)$ that depends on the velocity across the suspension V_s and a viscous band ε [15], as presented in Figure 1.

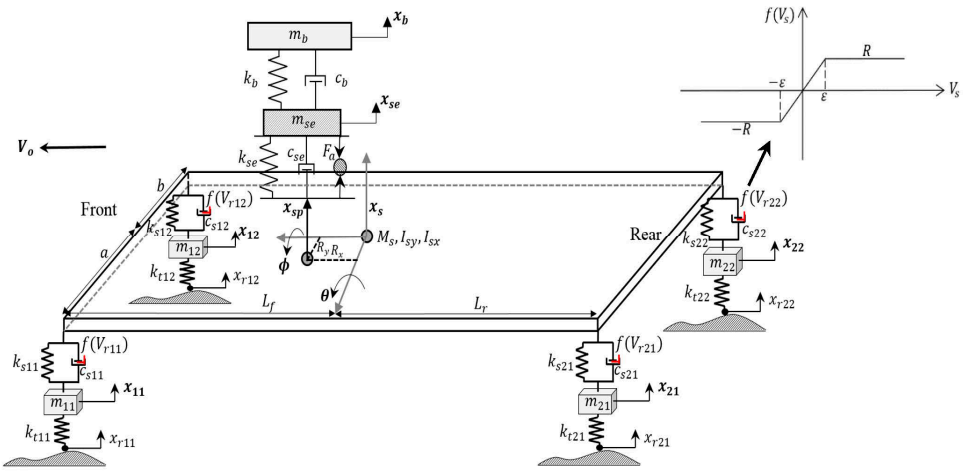

Figure 1. Full vehicle model.

1.2. Fuzzy Logic Controller

Generally, an FLC consists of four parts, as shown in Figure 2 [46]:

(1) A fuzzification interface, which changes the controller inputs to linguistic variables that can be utilised in the inference mechanism.
(2) A rule-base (RB), which is a set of linguistic ("if-then") rules that stores the knowledge of how to control the process.
(3) An inference mechanism, which uses the linguistic inputs and the RB to produce the control decision.
(4) A defuzzification interface, which converts the linguistic outputs into crisp ones.

Put simply, the output of each proposed FLC is the control force. However, the total number of inputs for each FLC is different. For instance, the FLS-FLC has only two inputs, as presented in Figure 3a. The FA-FLC requires four inputs, namely the displacements and velocities of the front left and right suspensions. Conversely, the number of inputs to the 4W-FLC are eight. However, the number of rules of the FLC depends on the number of input and output variables, as well as the number of their MFs. For example, assume that each input variable of the FA-FLC consists of five MFs, then a total of 625 rules are required to design its RB, and hence, there is an increase in the optimisation processing time and controller complexity.

Alternatively, the FA-FLC and 4W-FLC are assumed to be composed of sub-FLCs [38], such that each sub-FLC requires only two inputs, as shown in Figure 3b,c, respectively. Thus, the FA-FLC consists of two sub-FLCs, namely FA1-FLC and FA2-FLC, in which the former uses the preview information from the front-left vehicle suspension and generates the sub-control force F_{a1}. The latter utilises similar preview information, but from the front-right suspension, and produces the sub-control force F_{a2}, while the resultant control force is the sum of these forces. Similarly, the 4W-FLC has four sub-FLCs, each corresponding to each vehicle suspension. However, each sub-FLC has its own RB, thereby decreasing the computational time and reducing the overall RB size.

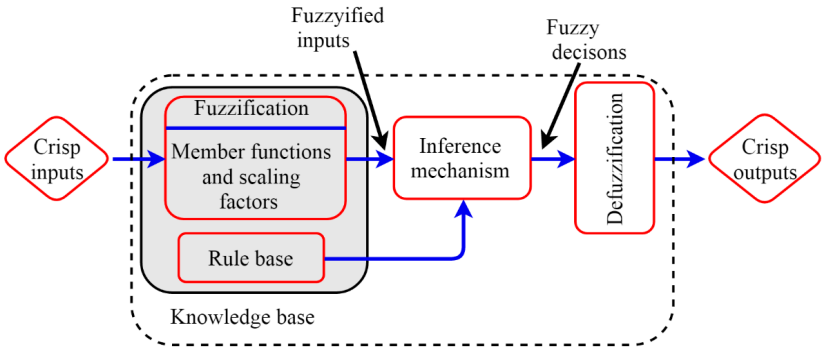

Figure 2. Fuzzy logic control (FLC) structure [47].

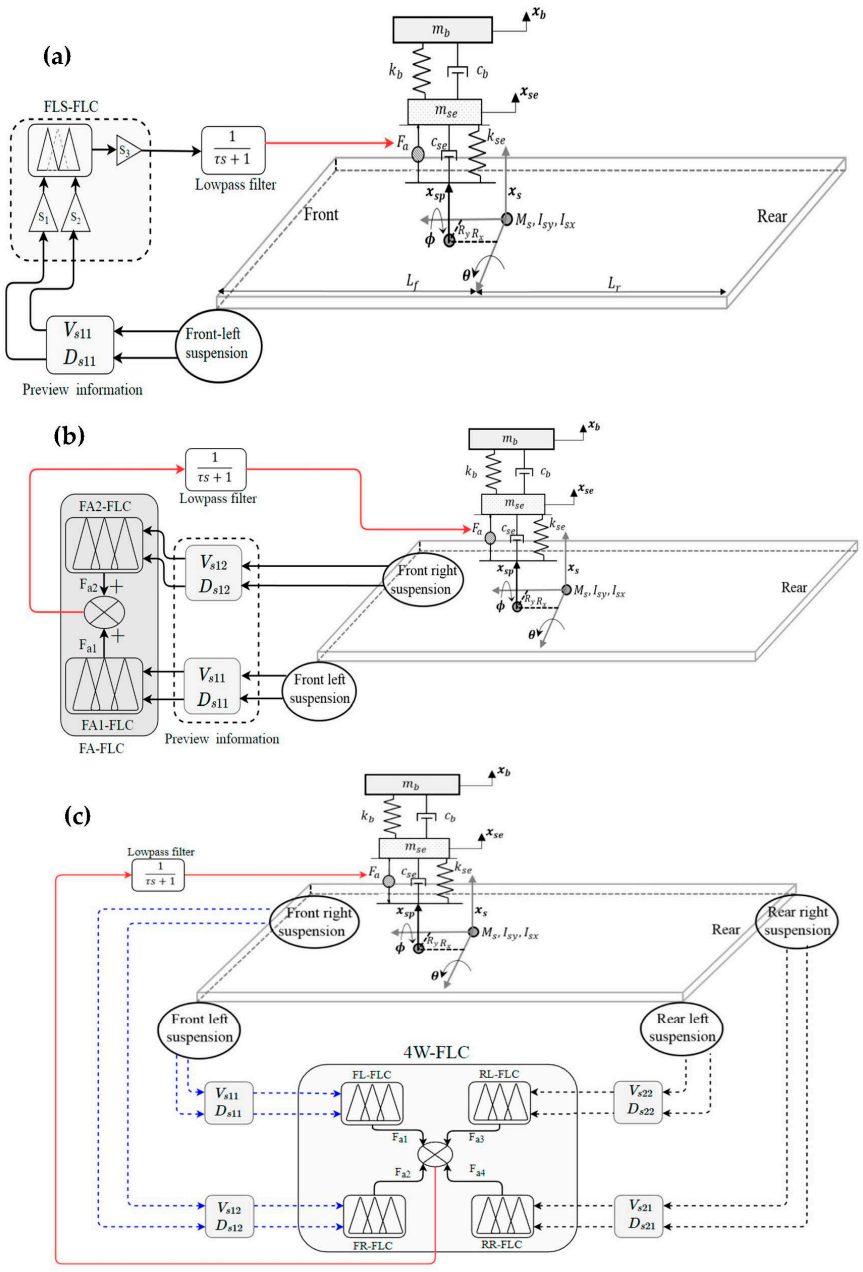

Figure 3. Schematic diagrams of: (**a**) FLS-FLC, (**b**) FA-FLC and (**c**) 4W-FLC.

1.3. Optimisation Process

The optimum FLC knowledge base is obtained sequentially through two stages, as shown in Figure 4a. Initially, the RB and scaling factors are optimised using assumed MFs. Then these are used in stage 2 to modify the parameters of the initial MFs. Hence, the output of the each proposed FLC is limited by the actuator force capacity. Thus, the output scaling factor S_3 of the FLS-FLC is constrained to be 1500.0 N. This ensures that the demand control force does not exceed the actuator force capacity, which is important in terms of stability and real-life implementation. However, this is not the case for the sub-FLCs, either in the FA-FLC or the 4W-FLC, which consist of different sub-FLCs. Nevertheless, the sum of all the output scaling factors of all the sub-FLCs in the main FLC is limited within the maximum allowable force. Moreover, the output of each FLC is filtered by a low-pass filter with a cut-off frequency of $f_n = 25$ Hz, in order to emulate the dynamics of the active force actuator, and also to reduce the effect of road-induced high-frequency content in the preview signal.

The MFs used in this study are of triangular shape, due to their simplicity and ease of adjustment, as well as offering the greatest output results with respect to other MF types [47]. Each input variable is assumed to be comprised of five linguistic degrees: negative big (NB), negative small (NS), zero (ZE), positive small (PS), and positive big (PB). The output fuzzy function consists of seven degrees: negative big (NP), negative medium (NM), negative small (NS), zero (ZE), positive small (PS), positive medium (PM), and big (PB), as shown in Figure 4b. Consequently, the RB of the FLS-FLC or any sub-FLCs is composed of 25 rules.

The rules and the scaling factors are formulated based on the PSO. For example, in stage 1 the size of the position vector of each particle in the PSO is 27, corresponding to the total number of design variables. The first 24 positions are assigned integer numbers from (1 to 7), which are equivalent to the linguistic degrees of the output variable. The remaining three design variables are allocated to the input and output scaling factors, respectively.

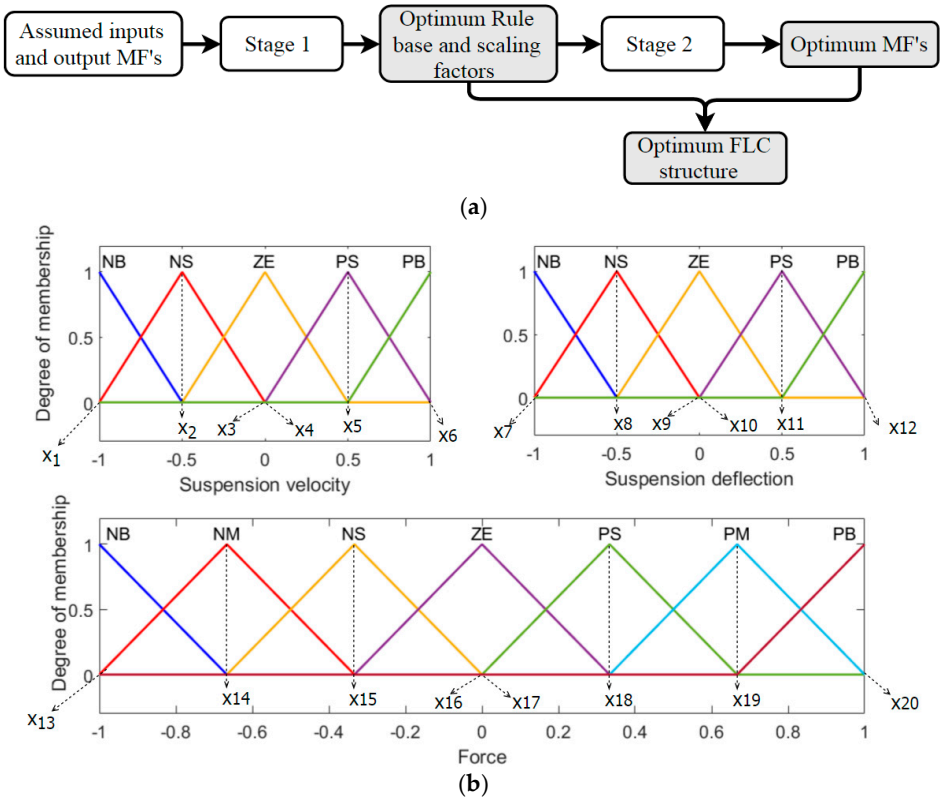

Figure 4. (**a**) Optimisation process of the FLC structure and (**b**) the membership functions (MFs) adjusting parameters.

The optimum RB and scaling factors are obtained in Stage 1 using the assumed MFs; then, in stage 2, the parameters of these MFs are modified, using the optimum RB and scaling factors. These parameters are adjusted based on the assumptions given in [38]. Thus, each input and output variable has six and eight MF parameters to be adjusted, respectively, as illustrated in Figure 4b.

Ride quality is related to both the magnitude and frequency content of the vertical vibration sensed by the human body, particularly over a frequency range of 4–8 Hz. Thus the seat effective amplitude transmissibility (SEAT) factor in the vertical direction was selected as the objective function in the optimisation process. It is defined as the ratio between the frequency-weighted root mean square (RMS) acceleration at the seat to that at the seat base [48], as follows:

$$SEAT = \frac{\left(\ddot{x}_{se,w}\right)_{rms}}{\left(\ddot{x}_{s,w}\right)_{rms}} \tag{9}$$

The subscript w in the previous formula indicates that the acceleration values are weighted according to the frequency weighted function W_k, as suggested by ISO 2631-1 [49] and shown in Figure 5. This scheme weights the human body's most sensitive frequency range (4–8 Hz) more heavily than other frequencies.

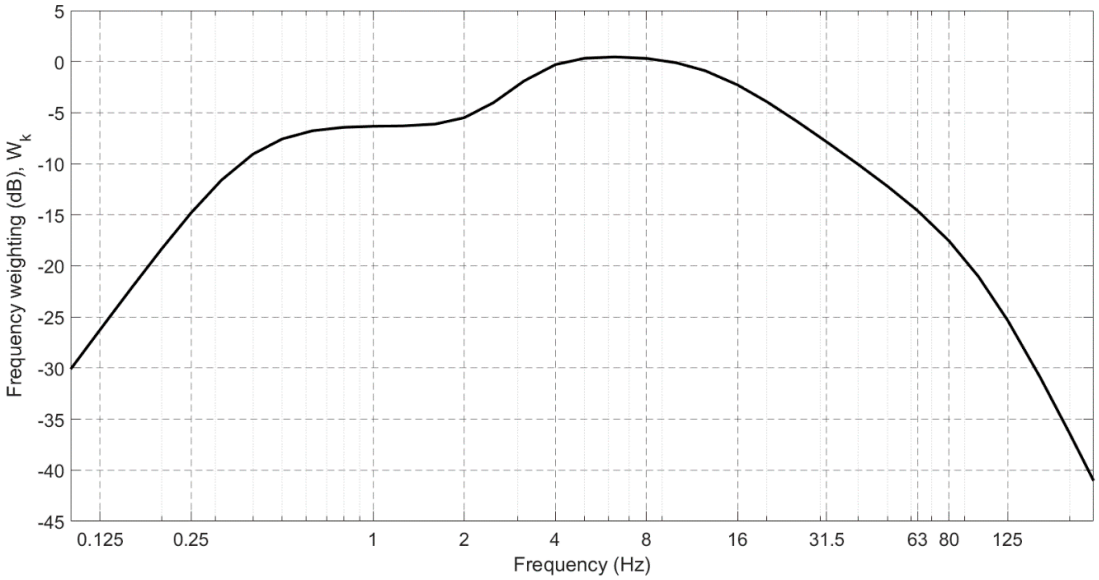

Figure 5. Frequency weighting function for the vertical vibration ISO 2361-1 [49].

Reducing the seat acceleration results in large seat suspension strokes, which are physically bounded [2]. Thus, this constraint is considered in the optimisation problem, such that the maximum allowable seat suspension travel ($x_{se,max}$) was assumed to be 45 mm.

The system was modelled using Simulink, and the optimisation problem was formulated in MATLAB and solved off-line, using the PSO and Fuzzy Logic toolboxes with a time step size of 0.001 s. Due to the fact that most road unevenness is best described by random profiles, which include the frequency range most sensitive to the human body in the vertical direction, a random road profile was selected in the optimisation process. The random road profile used in this study is of class E (very poor) road roughness according to the ISO-8606 standard [50], which was previously used by the authors in [34] with a vehicle forward speed of 60 km/h. In the optimisation process, the default MATLAB setting parameters of the PSO algorithm were used with a swarm size of 14. The type of fuzzy system used in this study is a Mamdani-type, and the centre of gravity method is used in the defuzzification process.

Moreover, the full vehicle model was excited at the left and right front wheels with different disturbances [51]. The disturbances at the rear wheels were similar to those at the front, with a time delay that depended on the vehicle wheel base and the vehicle speed.

To achieve realistic dynamic responses, the characteristics of the passive seat suspension (m_{se}, k_{se} and c_{se}), as well as the driver's body (k_b and c_b), were determined from experimental tests of a passive seat suspension with a dummy [34]. The parameters of the full vehicle model and the characteristics of the passive seat suspension, as well as those of the driver's body, are listed in Table 1.

Table 1. Parameters of the full vehicle model [52], passive seat suspension and driver's body.

Parameter		Value	Unit
M_s		1200.0	Kg
m_{ij}	$i, j = 1$ and 2	20.0	Kg
I_{sy}		2100.0	Kg·m^2
I_{sx}		460.0	Kg·m^2
K_{sij}	$(i, j = 1$ and $2)$	10.0	kN/m
c_{sij}	$(i, j = 1$ and $2)$	2000.0	N·s/m
K_{tij}	$(i, j = 1$ and $2)$	180.0	kN/m
L_f		1.011	m
L_r		1.803	m
a		0.761	kN·s/m
b		0.761	kN/m
R_x		0.3	m
R_y		0.25	m
R		22.0	N
ε		0.0012	m/s
m_{se}		5.0	Kg
m_b		55.25	Kg
c_{se}		2.10	kN·s/m
k_{se}		42.0	kN/m
c_b		0.9	kN·s/m
k_b		280.0	kN/m

After solving the optimisation problem for each FLC, the resulting optimum controller maps are presented in Figure 6. In addition, the demand control force of both the FLS-FLC and the FA-FLC were plotted, using contour plots as shown in Figure 7a,b, respectively. These maps encompass a very wide range of suspension operating conditions that are unlikely to be experienced during normal operation. From these figures, it can be observed that the output map of the FA1 is very similar to that of the FLS-FLC, with only small differences in the output force. In addition, the output force of the FLCs is zero when both the vehicle suspension displacement and velocity are zero.

The interpretation of these maps is not easy, as the control force is based on the vehicle suspension states and applied to the seat suspension, which is influenced by all four vehicle suspensions and vehicle body dynamics. Nevertheless, some cases can be explained; for example, in the case of FLS-FLC, when the vehicle suspension displacement and velocity are both NB (negative big) and the vehicle suspension is largely compressed, the seat suspension is also compressed, and a large positive actuator force is required to cancel this effect on the seat suspension, as shown in Figure 7a. Also, this is evident for the FA-FLC, as shown in Figure 7b.

To clarify these results further, the control force from FLS-FLC and the seat suspension force are compared when the vehicle is excited by a random road profile over a whole range of vehicle speeds, from 20 to 100 km/h (Figure 8). It is clear that when the vehicle suspension displacement and velocity is positive big, the control force is negative big, and vice versa. The same is true of the relationship between the seat suspension states and the control force.

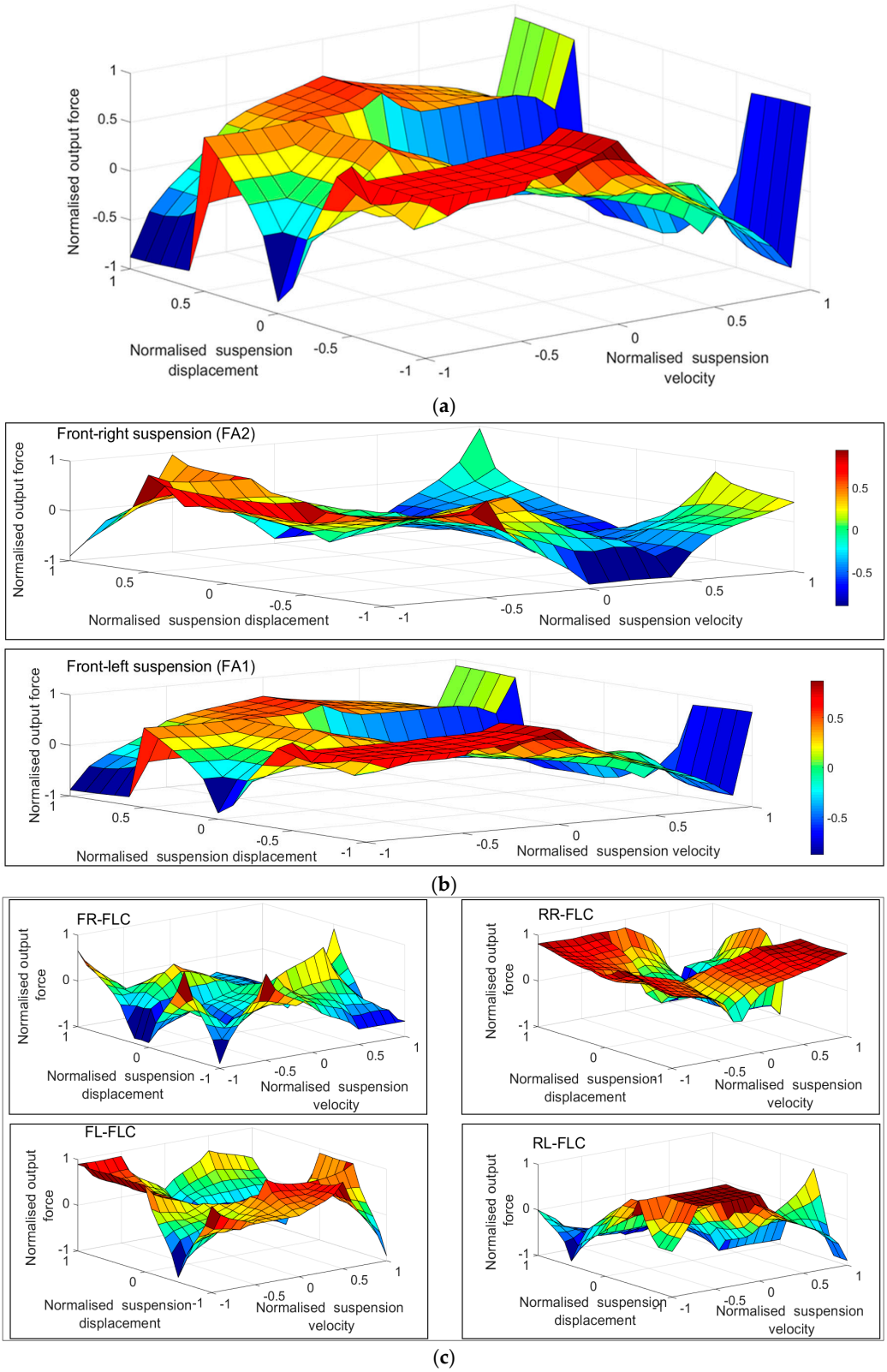

Figure 6. Optimum map for: (**a**) Front-left suspension (FLS-FLC), (**b**) front axle (FA-FLC), and (**c**) four wheels (4W-FLC).

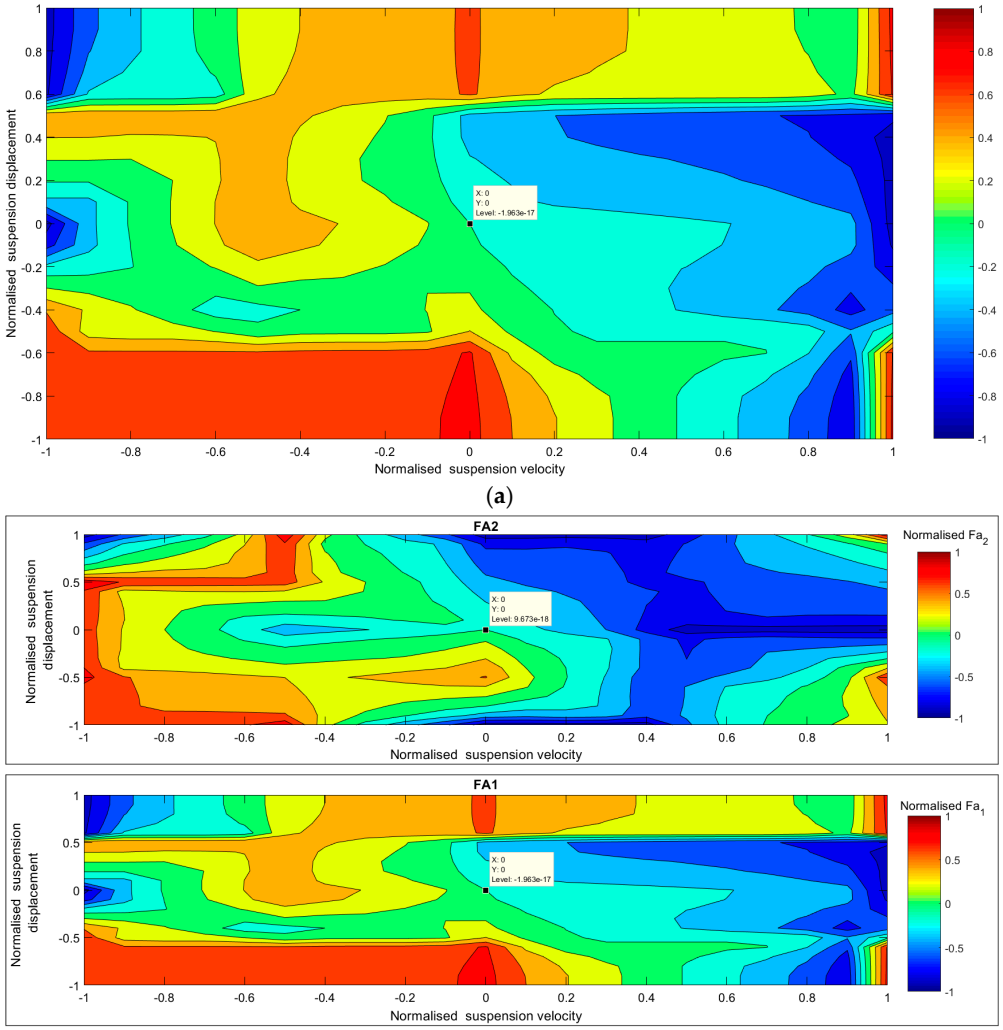

Figure 7. Contour plots of (**a**) the FLS-FLC map and (**b**) the FA-FLS map.

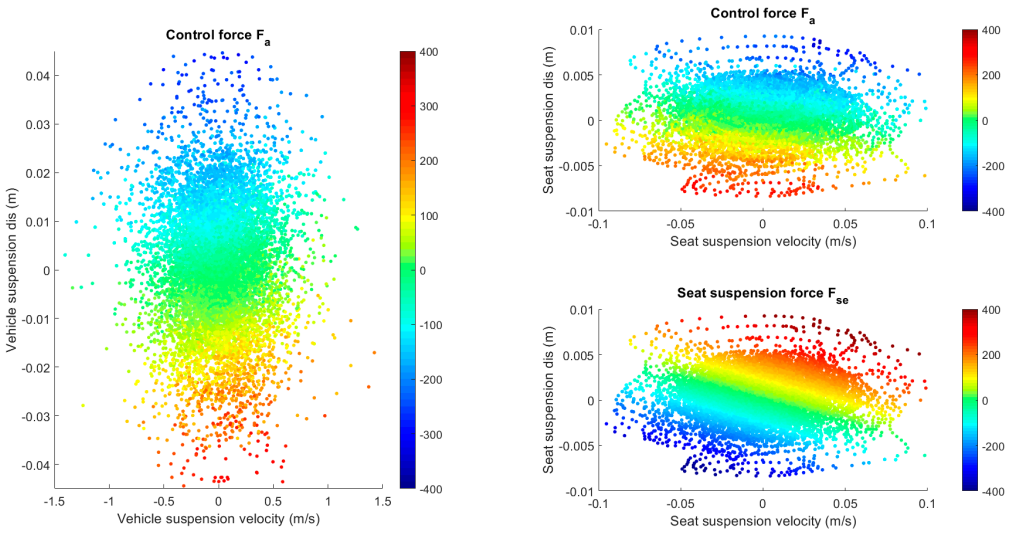

Figure 8. Contour plots of the seat suspension and control force of the FLS-FLC.

2. Simulation Analysis

2.1. Random Road

In this analysis, the full vehicle model was excited using an artificial random road profile of class E (very poor) according to the ISO 8608 standard, which has a road roughness of 256 $\times$ 10^{-6} m^3. For more details, refer to [34]. Figure 9 shows an example of this road input in the time domain at a vehicle speed of 60 km/h. For the sake of brevity, only the time domain responses of the active and passive seat suspensions at low and high forward vehicle speeds are presented, as shown in Figure 10. Moreover, the RMS values of the seat acceleration and seat suspension travel over the whole range of vehicle speeds are presented in Figure 11; due to the random nature of the road excitation, the simulations were performed 10 times for each vehicle speed over a time period of 20 s, and then an average was taken.

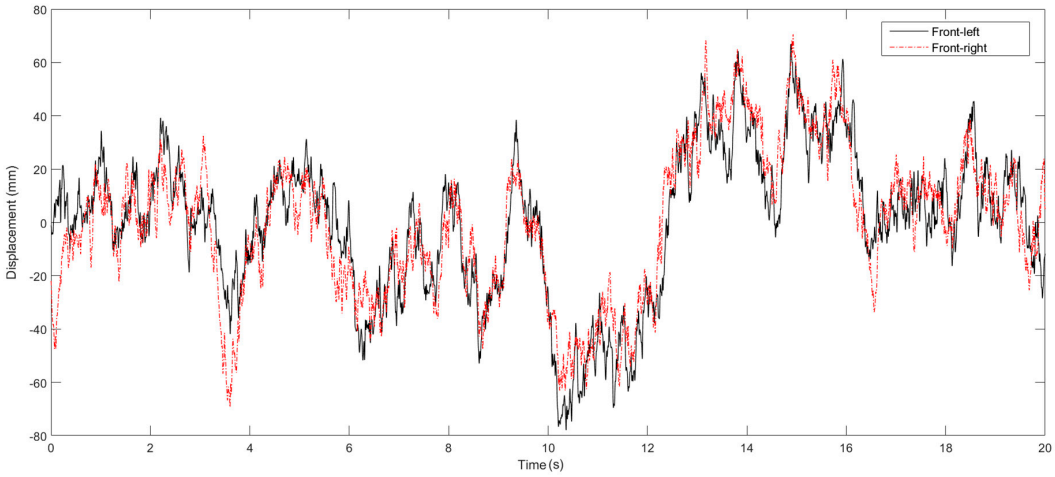

Figure 9. Road profile at a vehicle speed of 60 km/h.

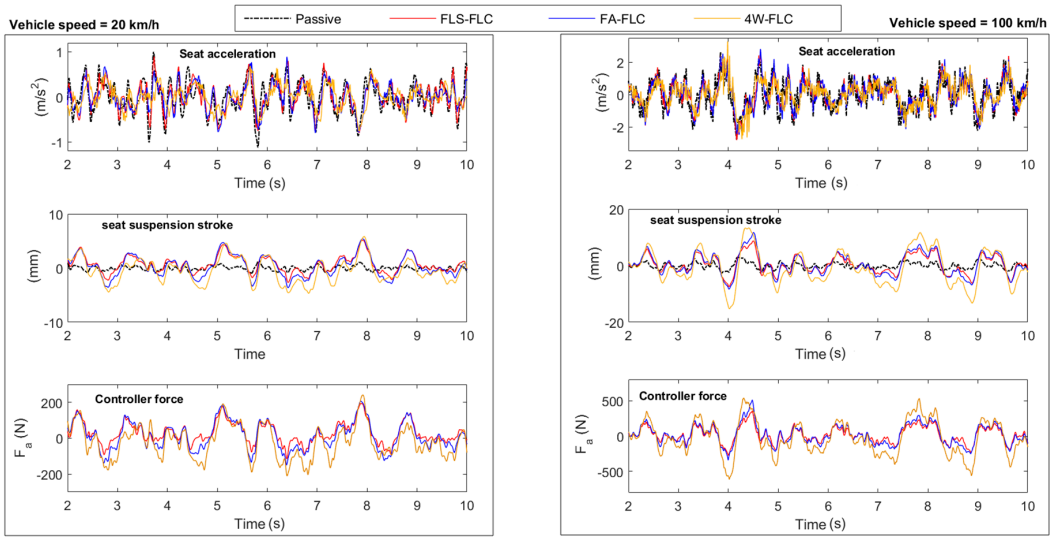

Figure 10. Time responses at low and high vehicle speeds.

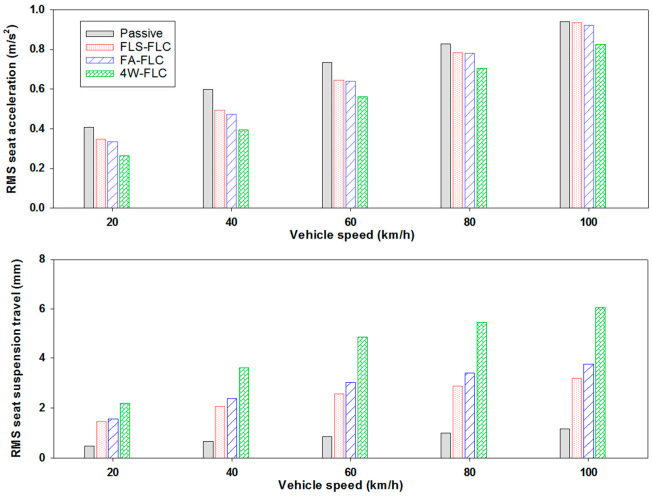

Figure 11. Comparison of ride comfort for passive and active seat suspension systems at different vehicle speeds.

From these figures, it can be seen that the controllers more effectively reduce the seat acceleration when compared with the passive system, with the 4W-FLC delivering the best performance, followed by the FA-FLC and the FLS-FLC, respectively. However, this improvement in the ride quality comes at the expense of increased seat suspension travel, although constraints for both this and the actuator force are satisfied.

It can be observed from Figure 12 that the active seat suspensions provide lower power spectral density (PSD) acceleration when compared with the passive system over a broadband frequency range, especially over the human body sensitive frequency range (4–8 Hz). However, this performance deteriorates at lower frequencies during high vehicle forward speeds. In general, the 4W-FLC demonstrates the best performance over a broadband frequency range, irrespective of the vehicle speed followed by the FA-FLC and the FLS-FLC.

Figure 13a,b shows that the proposed active seat suspensions significantly attenuate the vibration at the seat, as well as reduce the weighted RMS seat acceleration when compared with the passive seat suspension. At high speed, the active systems perform less well, although they are as good as the passive system throughout the speed range. The 4W-FLC provides the best vibration isolation performance, in which the transmitted vibration and the weighted RMS seat acceleration are reduced by at least 20% regardless of the vehicle speed, as shown in Figure 13c,d.

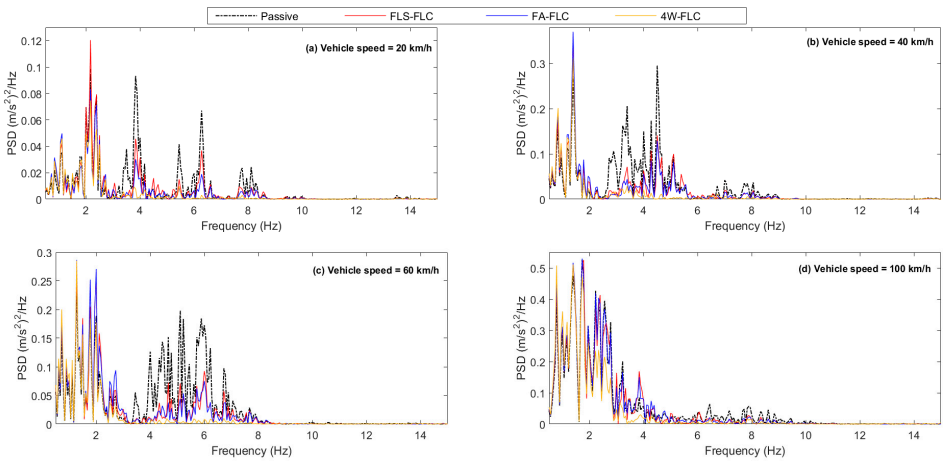

Figure 12. Power spectral densities (PSDs) of the seat acceleration at different vehicle speeds.

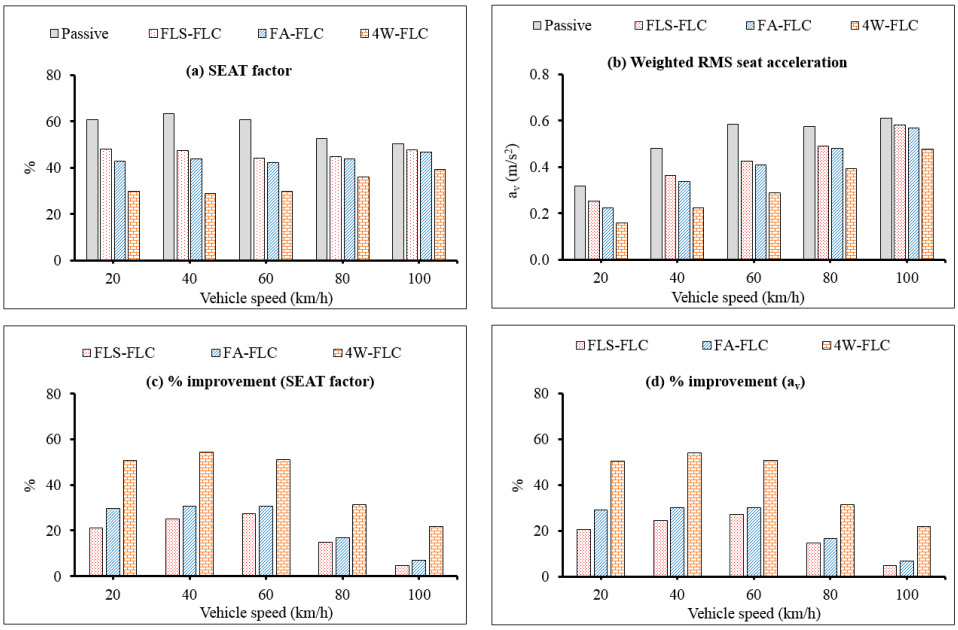

Figure 13. SEAT factor, weighted RMS seat acceleration and percentage improvements at different vehicle speeds.

Whilst the 4W-FLC is shown to be the best preview based controller for use in an active seat suspension, its real implementation is somewhat costly, as it requires instrumentation at each corner of the car. This can be partially overcome in a new controller, denoted as the "practical four wheel" (P4W) FLC, which is similar to the 4W-FLC, but uses fewer states. Specifically, this controller employs the same optimum sub-fuzzy logic controllers as the 4W-FLC. However, it requires only the states from the front suspensions as the required states from rear suspensions are hypothesised as a time delayed version of the measured states at the front, as illustrated in Figure 14. It should be noted that, due to this assumption, the performance of P4W-FLC in some maneuvers such as hard cornering will be compromised.

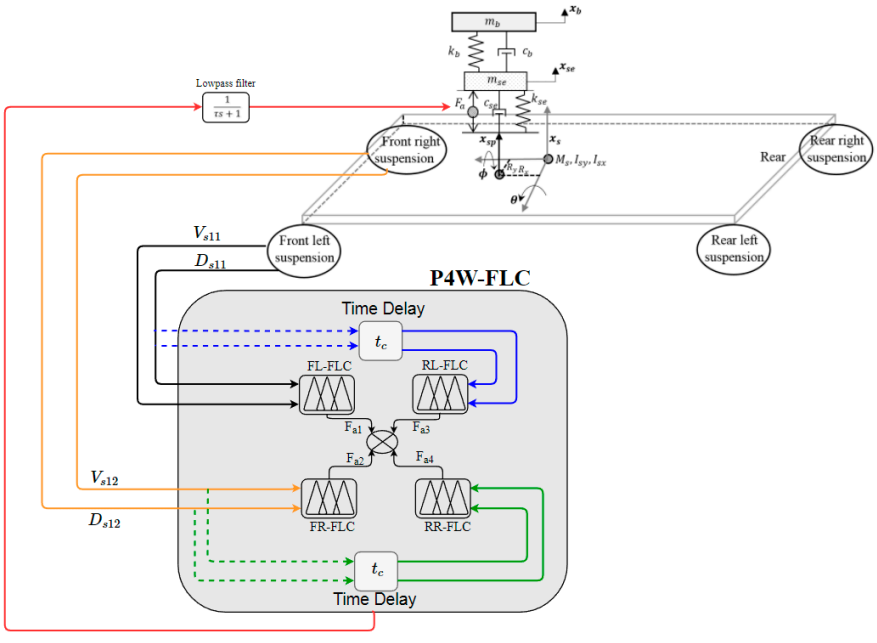

Figure 14. Schematic diagram of the P4W-FLC.

Figure 15 compares the seat acceleration PSD of the P4W-FLC and 4W-FLC active seats to those of the passive system. Clearly, the P4W-FLC is almost identical to the 4W-FLC regardless of the vehicle speed. Moreover, as shown in Figure 16, the P4W-FLC provides very similar vibration attenuation performance and weighted RMS seat acceleration to the 4W-FLC at the full range of vehicle speeds.

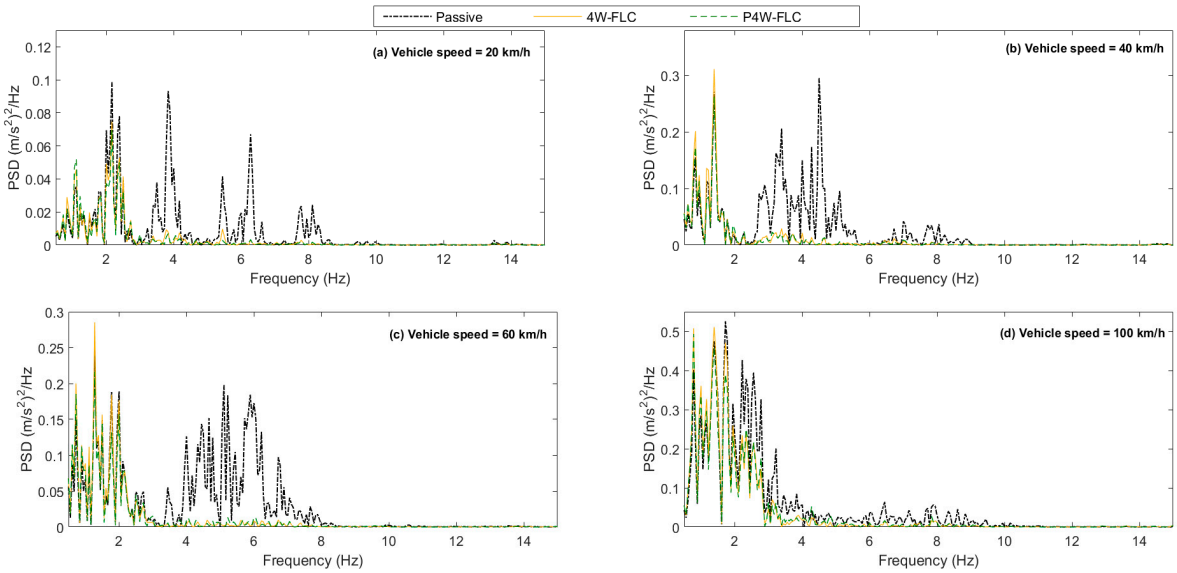

Figure 15. PSDs of the seat acceleration at different vehicle speeds.

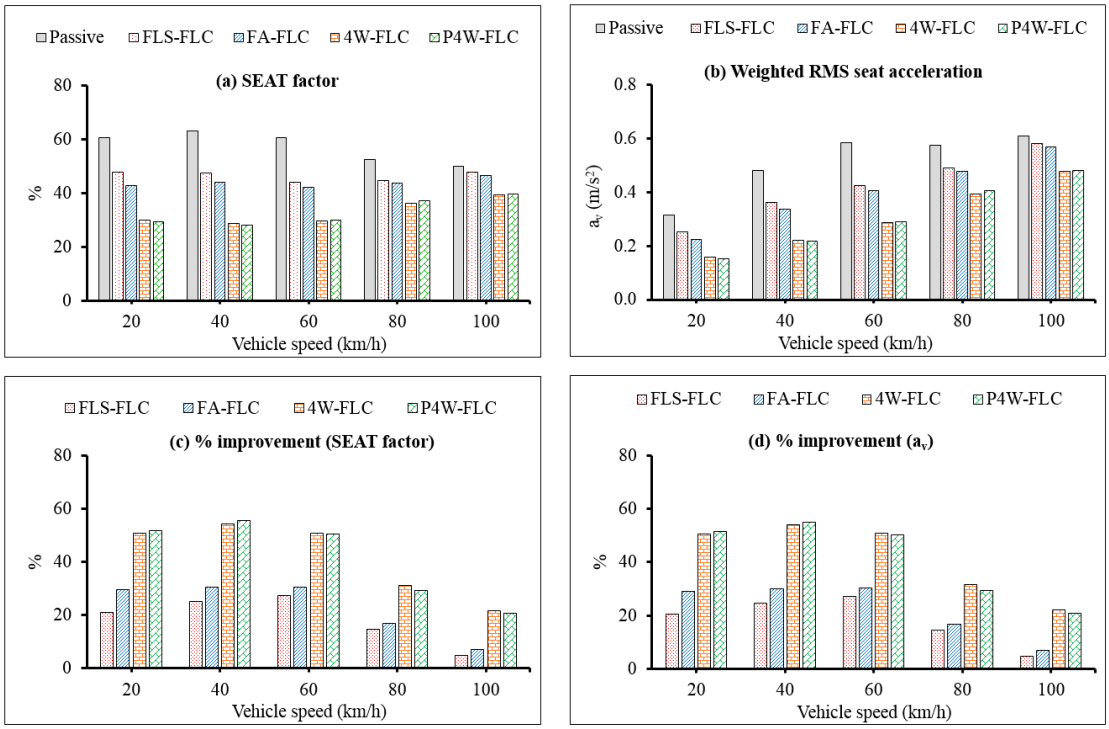

Figure 16. Seat effective amplitude transmissibility (SEAT) factor, weighted RMS seat acceleration, and percentage improvements at different vehicle speeds.

Figure 17 shows the frequency-weighted RMS acceleration of the active and passive seat suspensions with respect to the threshold limit values (TLVs), as suggested by the American Conference of Government Industrial Hygienists [53]. It can be seen that the active seat suspension, using any of the developed controllers, delivers a lower frequency-weighted RMS seat acceleration over the human body-sensitive frequency range, whereas the passive system exceeds the 16-hour working daily exposure limit. Once again, the performance of both the LFS-FLC and FA-FLC are reduced at high vehicle speeds, at which the FA-FLC performs very similarly to the FLS-FLC. In fact, the 4W-FLC provides the best performance regardless of vehicle speed, while the P4W-FLC delivers almost identical results to the 4W-FLC at a reduced cost, in terms of state measurements.

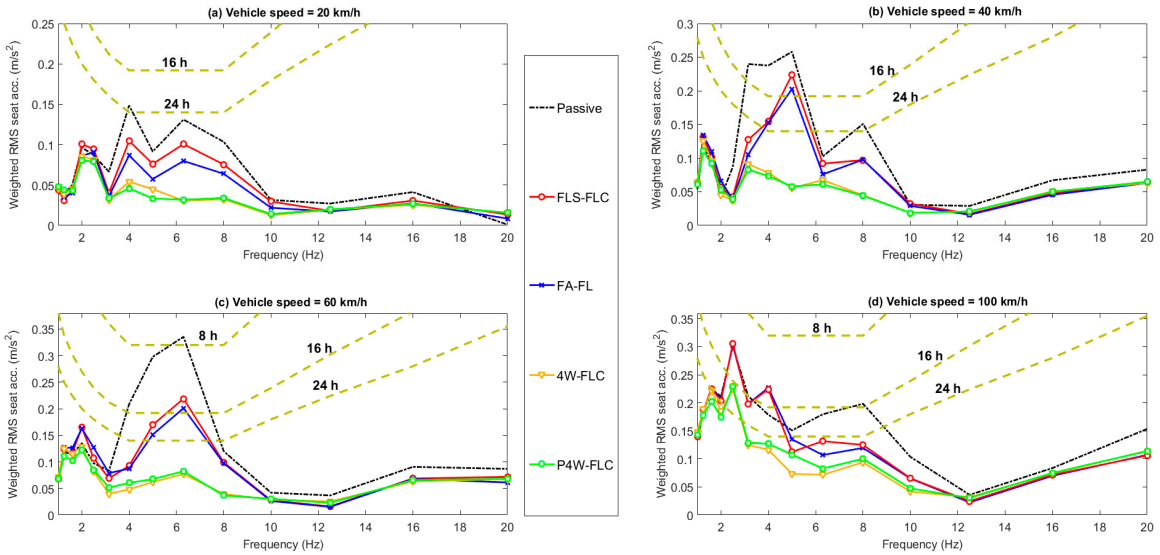

Figure 17. Health risk assessment of the passive and proposed active seat suspensions at different vehicle speeds.

2.2. Parameter Uncertainties

In order to investigate the robustness of the proposed active seat suspension systems, the systems' performance was evaluated when subject to variations in the system parameters and operating conditions. The most varying parameters for an active seat suspension are the vehicle speed and the driver's weight, and thus the performance of the developed FLCs' active seat suspension under the variation in these parameters was examined in terms of the SEAT factor and the weighted RMS seat acceleration. Due to the nature of a random road, the simulations were carried out 10 times over a period of 20 s, and the average values were taken. Figure 18 shows the sensitivity maps of the SEAT factor for the passive and active seat suspension systems, subject to variations in the vehicle speed and the driver's weight. It is clear that the isolation performance of the passive seat suspension is sensitive to changes in both parameters. Notably, heavy drivers are exposed to less vibration energy than lighter ones, regardless of the vehicle speed. On the other hand, the vibration isolation performance of the developed FLCs is less sensitive to passenger weight variations, in which the 4W-FLC and P4W-FLC provide the highest robustness level.

Figure 18 also reveals that the ride comfort level of the passive seat suspension is highly sensitive to variations in both the driver's weight and the vehicle speed, in which light drivers are subject to the most discomfort when driving at high speeds. In comparison, the FLCs were only slightly affected by these changes, especially at low and intermediate vehicle speeds. Once again, the 4W-FLC and P4W-FLC provide the highest robustness level, compared with the FLS-FLC and FA-FLC.

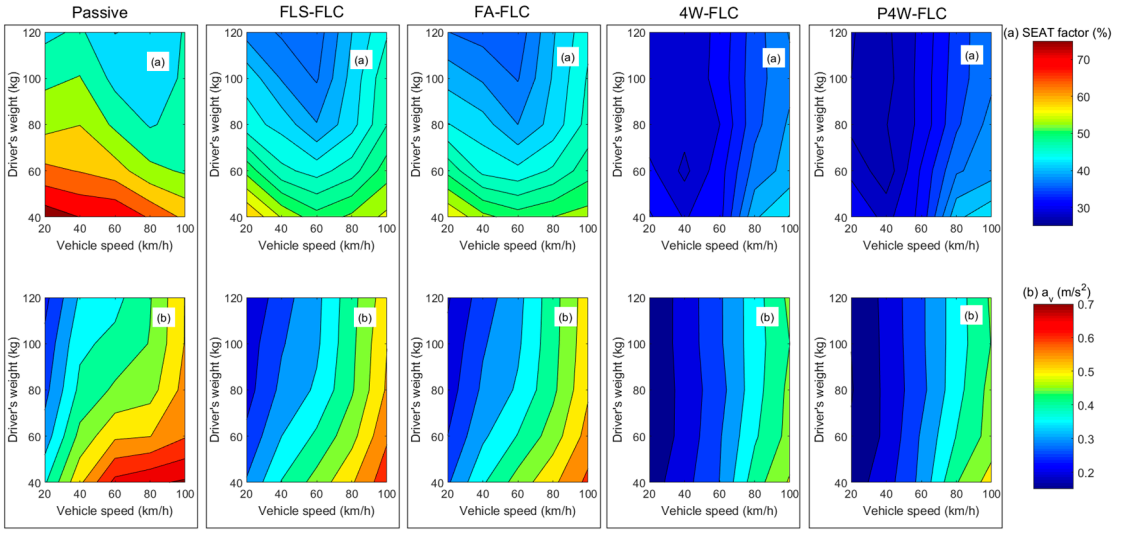

Figure 18. Sensitivity of the passive and active seat suspension performance to variations in the driver's weight and vehicle speed.

2.3. Road "Bump" Input

Figure 19a shows the bump road profile used to excite the full vehicle model [54]. Figure 19b,c shows the superior ability of the proposed controllers to reduce the seat acceleration when compared with the passive system, without exceeding the seat suspension travel limit. However, the active seat suspension using the P4W-FLC shows a peak acceleration value at approximately 0.5 s, which may be due to the fact that the suspension states from the rear axle used in this controller are approximated from the front axle, which introduces compromises in the controller that are reflected in high frequency seat actuator force inputs and associated seat accelerations, especially when using a very severe bump road profile.

Once again, the 4W-FLC and P4W-FLC show very similar results, reducing the RMS value of seat acceleration from 1.031 m/s^2 with the passive system to be less than 0.75 m/s^2, as presented in Table 2.

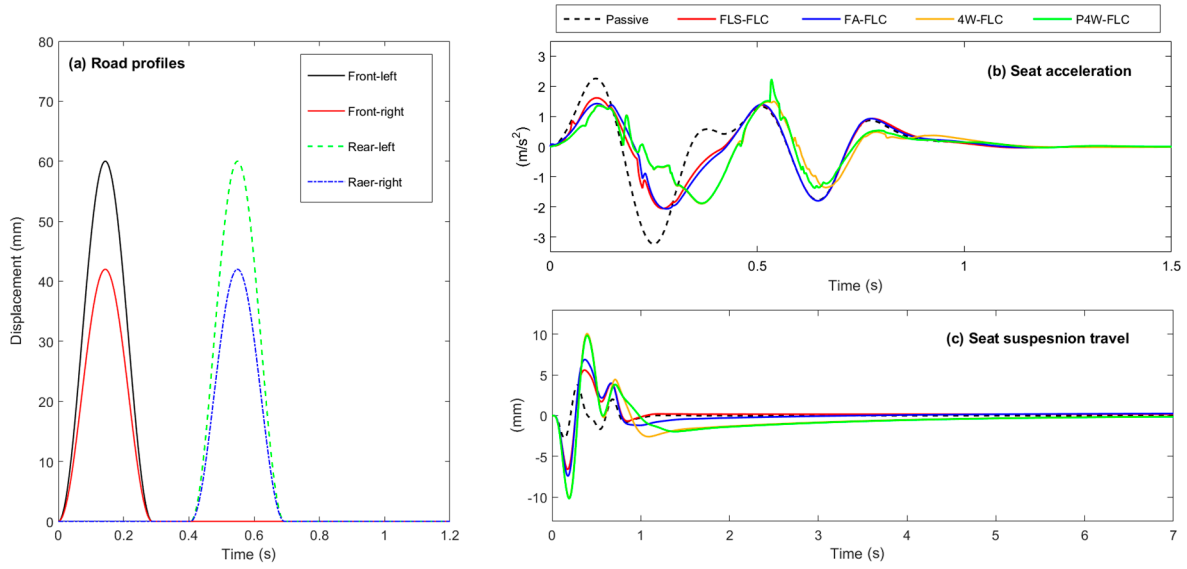

Figure 19. Time responses under a bump road profile.

Table 2. Time responses characteristics of the proposed controllers under a bump road profile.

System	Seat Acceleration		Seat Suspension Travel	
	RMS (m/s^2)	Peak (m/s^2)	RMS (mm)	Peak (mm)
Passive	1.031	3.236	1.238	3.749
FLS-FLC	0.825	2.055	2.720	6.595
FA-FLC	0.802	2.060	3.057	11.840
4W-FLC	0.728	1.895	4.349	10.090
P4W-FLC	0.734	2.228	4.192	10.183

3. Conclusions

In this paper, three novel and cost-effective FL controllers for an active seat suspension have been developed, which use inexpensive and available preview information from the vehicle suspensions while satisfying the physical system constraints at a range of different operational conditions. The simulation results indicated that the controllers significantly improve ride comfort compared with the passive system. The 4W-FLC shows the best performance regardless of the vehicle speed. Interestingly, the P4W-FLC performs very similarly to the 4W-FLC, and requires fewer measured system states, thus it is a practical and cost-effective system that improves ride comfort and reduces driver fatigue.

Acknowledgments: This research received no specific grant from any funding agency in the public, commercial, or not for-profit sectors: This work was supported by the University of Bath.

Author Contributions: This work was undertaken by Abdulaziz Alfadhli as part of a three year PhD, supervised by Jocelyn Darling and Andrew J. Hillis who initially conceived and designed the program of work. Abdulaziz Alfadhli developed the simulation model and produced the theoretical results which were then interpreted by all three authors. The paper was jointly written by the three researchers.

Conflicts of Interest: The authors declare no conflict of interest in preparing this article.

Notation

4W	Four wheel
4W-FLC	Four wheel fuzzy logic controller
ACGIH	American Conference of Government Industrial Hygienists
DOFs	Degrees of freedom
FA	Front axle
FA-FLC	Front axle fuzzy logic controller
FLC	Fuzzy logic controller
FLS	Front left suspension
FLS-FLC	Front left suspension fuzzy logic controller
ISO	International standard organization
LMS	Least Mean squares
MFs	Membership functions
P4W-FLC	Practical four wheel fuzzy logic controller
PSD	Power spectral density
PSO	Particle swarming optimisation
RB	Rule base
RMS	Root mean square
SEAT	Seat Effective Amplitude Transmissibility factor
TLVs	Threshold limit values

Symbol	Description
a_v	Frequency-weighted RMS acceleration
W_i	Frequency-weighting value at the centre frequency
$(\ddot{x}_{s,w})_{rms}$	Weighted root mean square vertical acceleration at the seat's base
$(\ddot{x}_{se,w})_{rms}$	Weighted root mean square of the vertical seat acceleration
$(x_{se} - x_s)_{max}$	Maximum seat stroke
$(x_{se} - x_s)_{min}$	Minimum seat stroke
$\ddot{x}_s$	Vertical acceleration of the sprung mass
$\ddot{x}_{se}$	Vertical acceleration of the seat
$\ddot{x}_{us}$	Vertical acceleration of the usprung mass
D_{sij}	Vehicle suspension displacement i and $j = 1,\ 2$
F_a	Actuator control force
F_s	Vehicle suspension dynamic force
F_{se}	Seat suspension dynamic force
I_{sx}	Moment of inertia in the longitudinal direction
I_{sy}	Moment of inertia in the lateral direction
R_x	Lateral distance from the driver's seat to C.G
R_y	Longitudinal distance from the driver's to C.G
V_{sij}	Vehicle suspension velocity, i and $j = 1,\ 2$
$V_o,\ V$	Forward vehicle speed
D_{sij}	Vehicle suspension displacement, i and $j = 1,\ 2$
c_s	Damping coefficient of the vehicle suspension
c_{se}	Damping coefficient of the seat suspension
k_s	Stiffness of the vehicle suspension
k_{se}	Stiffness of the seat suspension
k_t	Stiffness of the tyre
m_b	Human body mass
k_b	Human body spring rate
c_b	Damping coefficient of human body
$x_{se,max}$	maximum allowable seat stroke
$x_{se,min}$	minimum allowable seat stroke
x_{se}	vertical displacement of the seat
x_{us}	vertical displacement of the usprung mass
$\ddot{\theta}$	Pitch angular acceleration
$\ddot{\phi}$	Roll angular acceleration
R	Dry friction force limit
$f(V_s)$	Dry friction force (full vehicle model)
ε	Viscous band
θ	Pitch rotation angle
f_n	Cut-off frequency
ϕ	Roll rotation angle

References

1. Anna, D.H. *The Occupational Environment: Its Evaluation, Control and Management*; American Industrial Hygiene Association: Dayton, OH, USA, 2011.
2. Maciejewski, I.; Meyer, L.; Krzyzynski, T. Modelling and multi-criteria optimisation of passive seat suspension vibro-isolating properties. *J. Sound Vib.* **2009**, *324*, 520–538. [CrossRef]
3. Karnopp, D. Active and semi-active vibration isolation. *Trans. ASME J. Vib. Acoust.* **1995**, *117*, 177–185. [CrossRef]
4. Kawana, M.; Shimogo, T. Active suspension of truck seat. *Shock Vib.* **1998**, *5*, 35–41. [CrossRef]
5. Gu, Z.; Zhao, Y.; Gu, Z.; Fei, S.; Tian, E. Robust control of automotive active seat-suspension system subject to actuator saturation. *J. Dyn. Syst. Meas. Control Trans. ASME* **2014**, *136*. [CrossRef]

6. Ning, D.; Sun, S.; Li, H.; Du, H.; Li, W. Active control of an innovative seat suspension system with acceleration measurement based friction estimation. *J. Sound Vib.* **2016**, *384*, 28–44. [CrossRef]
7. Sun, W.; Li, J.; Zhao, Y.; Gao, H. Vibration control for active seat suspension systems via dynamic output feedback with limited frequency characteristic. *Mechatronics* **2011**, *21*, 250–260. [CrossRef]
8. Gan, Z.; Hillis, A.J.; Darling, J. Adaptive control of an active seat for occupant vibration reduction. *J. Sound Vib.* **2015**, *349*, 39–55. [CrossRef]
9. Hillis, A.J. Adaptive Control of Active Engine Mounts. Ph.D. Thesis, University of Bristol, Bristol, UK, 2005.
10. Sezgin, A.; Hacioglu, Y.; Yagiz, N. Sliding Mode Control for Active Suspension System with Actuator Delay. World Academy of Science, Engineering and Technology. *Int. J. Mech. Aerosp. Ind. Mechatron. Manuf. Eng.* **2016**, *10*, 1356–1360.
11. Yagiz, N.; Yuksek, I.; Sivrioglu, S. Robust Control of Active Suspensions for a Full Vehicle Model Using Sliding Mode Control. *JSME Int. J. Ser. C Mech. Syst. Mach. Elem. Manuf.* **2000**, *43*, 253–258. [CrossRef]
12. Yoshimura, T.; Kume, A.; Kurimoto, M.; Hino, J. Construction of an active suspension system of a quarter car model using the concept of sliding mode control. *J. Sound Vib.* **2001**, *239*, 187–199. [CrossRef]
13. Eski, I.; Yıldırım, Ş. Vibration control of vehicle active suspension system using a new robust neural network control system. *Simul. Model. Pract. Theory* **2009**, *17*, 778–793. [CrossRef]
14. Rao, M.V.C.; Prahlad, V. A tunable fuzzy logic controller for vehicle-active suspension systems. *Fuzzy Sets Syst.* **1997**, *85*, 11–21. [CrossRef]
15. Guclu, R. Fuzzy Logic Control of Seat Vibrations of a Non-Linear Full Vehicle Model. *Nonlinear Dyn.* **2005**, *40*, 21–34. [CrossRef]
16. Hurel, J.; Mandow, A.; García-Cerezo, A. Tuning a fuzzy controller by particle swarm optimization for an active suspension system. In Proceedings of the IECON 2012 38th Annual Conference on IEEE Industrial Electronics Society, Montreal, QC, Canada, 25–28 October 2012; pp. 2524–2529.
17. Moon, S.Y.; Kwon, W.H. Genetic-based fuzzy control for half-car active suspension systems. *Int. J. Syst. Sci.* **1998**, *29*, 699–710. [CrossRef]
18. Sharkawy, A.B. Fuzzy and adaptive fuzzy control for the automobiles' active suspension system. *Veh. Syst. Dyn.* **2005**, *43*, 795–806. [CrossRef]
19. Taskin, Y.; Hacioglu, Y.; Yagiz, N. The use of fuzzy-logic control to improve the ride comfort of vehicles. *Strojniski Vestn.* **2007**, *53*, 233–240.
20. Taskin, Y.; Hacioglu, Y.; Yagiz, N. Experimental evaluation of a fuzzy logic controller on a quarter car test rig. *J. Braz. Soc. Mech. Sci. Eng.* **2017**, *39*, 2433–2445. [CrossRef]
21. Akbari, A.; Koch, G.; Pellegrini, E.; Spirk, S.; Lohmann, B. Multi-objective preview control of active vehicle suspensions: Experimental results. In Proceedings of the IEEE 2nd International Conference on Advanced Computer Control (ICACC), Shenyang, China, 27–29 March 2010; pp. 497–502.
22. El Madany, M.; Abduljabbar, Z.; Foda, M. Optimal preview control of active suspensions with integral constraint. *Modal Anal.* **2003**, *9*, 1377–1400. [CrossRef]
23. El Madany, M.M.; Al Bassam, B.A.; Fayed, A.A. Preview control of slow-active suspension systems. *J. Vib. Control* **2011**, *17*, 245–258. [CrossRef]
24. El Madany, M.M. Control and evaluation of slow-active suspensions with preview for a full car. *Math. Probl. Eng.* **2012**, *2012*. [CrossRef]
25. HAĆ, A. Optimal Linear Preview Control of Active Vehicle Suspension. *Veh. Syst. Dyn.* **1992**, *21*, 167–195. [CrossRef]
26. Kitching, K.J.; Cebon, D.; Cole, D.J. An experimental investigation of preview control. *Veh. Syst. Dyn.* **1999**, *32*, 459–478. [CrossRef]
27. Li, P.; Lam, J.; Cheung, K.C. Multi-objective control for active vehicle suspension with wheelbase preview. *J. Sound Vib.* **2014**, *333*, 5269–5282. [CrossRef]
28. Nagiri, S.; Doi, S.; Shoh-no, S.; Hiraiwa, N. *Improvement of Ride Comfort by Preview Vehicle-Suspension System*; SAE Technical Paper; SAE: Warrendale, PA, USA, 1992.
29. Roh, H.-S.; Park, Y. Observer-based wheelbase preview control of active vehicle suspensions. *J. Mech. Sci. Technol.* **1998**, *12*, 782–791. [CrossRef]
30. Bender, E.K. Optimum linear preview control with application to vehicle suspension. *J. Basic Eng.* **1968**, *90*, 213–221. [CrossRef]

31. Arunachalam, K.; Jawahar, P.M.; Tamilporai, P. *Active Suspension System with Preview Control—A Review*; SAE Technical Paper; SAE: Warrendale, PA, USA, 2003.
32. Sarami, S. *Development and Evaluation of a Semi-Active Suspension System for Full Suspension Tractors*; Fachbereich Konstruktion von Maschinensystemen: Berlin, Germany, 2009. Available online: https://opus4.kobv.de/opus4-tuberlin/files/2402/sarami_shahriar.pdf (accessed on 22 September 2017).
33. Alvanagh, A.A. Multi-Objective H∞/GH2 Preview Control of Active Vehicle Suspensions. Ph.D. Thesis, Department of Control Engineering, Munich Polytechnic University, Munich, Germany, 2008. Available online: http://citeseerx.ist.psu.edu/viewdoc/download?doi=10.1.1.428.480&rep=rep1&type=pdf (accessed on 14 July 2017).
34. Alfadhli, A.; Darling, J.; Hillis, A.J. The control of an active seat with vehicle suspension preview information. *J. Vib. Control* **2017**, 1–15. [CrossRef]
35. Chiou, J.-S.; Tsai, S.-H.; Liu, M.-T. A PSO-based adaptive fuzzy PID-controllers. *Simul. Model. Pract. Theory* **2012**, *26*, 49–59. [CrossRef]
36. Pishkenari, H.N.; Mahboobi, S.H.; Alasty, A. Optimum synthesis of fuzzy logic controller for trajectory tracking by differential evolution. *Sci. Iran.* **2011**, *18*, 261–267. [CrossRef]
37. Chiou, J.-S.; Liu, M.-T. Using fuzzy logic controller and evolutionary genetic algorithm for automotive active suspension system. *Int. J. Automot. Technol.* **2009**, *10*, 703. [CrossRef]
38. Kaldas, M.; Caliskan, K.; Henze, R.; Küçükay, F. Preview Enhanced Rule-Optimized Fuzzy Logic Damper Controller. *SAE Int. J. Passeng. Cars Mech. Syst.* **2014**, *7*, 804–815. [CrossRef]
39. Montazeri-Gh, M.; Soleymani, M. Genetic optimization of a fuzzy active suspension system based on human sensitivity to the transmitted vibrations. *Proc. Inst. Mech. Eng. Part J. Autom. Eng.* **2008**, *222*, 1769–1780. [CrossRef]
40. Cao, J.; Li, P.; Liu, H.; Brown, D. Adaptive fuzzy controller for vehicle active suspensions with particle swarm optimization. In Proceedings of the Seventh International Symposium on Instrumentation and Control Technology, Beijing, China, 13 October 2008; p. 712922.
41. Rajeswari, K.; Lakshmi, P. PSO optimized fuzzy logic controller for active suspension system. In Proceedings of the IEEE International Conference on Advances in Recent Technologies in Communication and Computing (ARTCom), Kottayam, India, 16–17 October 2010; pp. 278–283.
42. Bingül, Z.; Karahan, O. A Fuzzy Logic Controller tuned with PSO for 2 DOF robot trajectory control. *Expert Syst. Appl.* **2011**, *38*, 1017–1031. [CrossRef]
43. Lazinica, A. *Particle Swarm Optimization*; In-Tech Kirchengasse: Graz, Austria, 2009. Available online: http://personnel.sju.edu.tw/%E6%94%B9%E5%96%84%E5%B8%AB%E8%B3%87%E7%A0%94%E7%A9%B6%E6%88%90%E6%9E%9C/98%E5%B9%B4%E5%BA%A6/%E8%91%97%E4%BD%9C/86.pdf (accessed on 23 January 2017).
44. Shi, Y. Particle swarm optimization: Developments, applications and resources. In Proceedings of the IEEE Congress on Evolutionary Computation, Seoul, Korea, 27–30 May 2001; pp. 81–86.
45. Bouazara, M.; Richard, M.J.; Rakheja, S. Safety and comfort analysis of a 3-D vehicle model with optimal non-linear active seat suspension. *J. Terramechanics* **2006**, *43*, 97–118. [CrossRef]
46. Passino, K.M.; Yurkovich, S. *Fuzzy Control Menlo Park*; Addison-Wesley: Harlow, CA, USA, 1998; ISBN 978-0-201-18074-9.
47. Zhao, J.; Bose, B.K. Evaluation of membership functions for fuzzy logic controlled induction motor drive. In Proceedings of the IEEE 28th Annual Conference of the Industrial Electronics Society (IECON 2002), Sevilla, Spain, 5–8 November 2002; pp. 229–234.
48. Griffin, M. *Handbook of Human Vibration*; Academic Press: London, UK, 1990.
49. ISO 2631-1:1997. *Mechanical Vibration and Shock—Evaluation of Human Exposure to Whole-Body Vibration—Part 1: General Requirements*; ISO: Geneva, Switzerland, 1997; p. 31.
50. ISO 8608:1995. Mechanical Vibration—Road Surface Profiles—Reporting of Measured Data. Available online: http://www.iso.org/iso/catalogue_detail.htm?csnumber=15913 (accessed on 10 January 2017).
51. Ren, H.B.; Chen, S.Z.; Wu, Z.C. Model of excitation of random road profile in time domain for a vehicle with four wheels. In Proceedings of the 2011 International Conference on Mechatronic Science, Electric Engineering and Computer (MEC), Jilin, China, 19–22 August 2011; pp. 2332–2335.
52. Du, H.; Li, W.; Zhang, N. Integrated seat and suspension control for a quarter car with driver model. *IEEE Trans. Veh. Technol.* **2012**, *61*, 3893–3908.

53. *Threshold Limit Values (TLVs) for Chemical Substances and Physical Agents and Biological Exposure Indices (BEIs)*; American Conference of Governmental Industrial Hygienists (ACGIH): Cincinnati, OH, USA, 2002; pp. 124–131.
54. D'Amato, F.J.; Viassolo, D.E. Fuzzy control for active suspensions. *Mechatronics* **2000**, *10*, 897–920. [CrossRef]